Deep Convective System Evolution over Africa and the Tropical Atlantic

JOANNA M. FUTYAN

Department of Applied Mathematics and Applied Physics, and Institute for Space Studies, Columbia University, New York, New York

ANTHONY D. DEL GENIO

NASA Goddard Institute for Space Studies, New York, New York

(Manuscript received 27 June 2006, in final form 21 February 2007)

ABSTRACT

In the tropical African and neighboring Atlantic region there is a strong contrast in the properties of deep convection between land and ocean. Here, satellite radar observations are used to produce a composite picture of the life cycle of convection in these two regions. Estimates of the broadband thermal flux from the geostationary *Meteosat-8* satellite are used to identify and track organized convective systems over their life cycle. The evolution of the system size and vertical extent are used to define five life cycle stages (warm and cold developing, mature, cold and warm dissipating), providing the basis for the composite analysis of the system evolution. The tracked systems are matched to overpasses of the Tropical Rainfall Measuring Mission satellite, and a composite picture of the evolution of various radar and lightning characteristics is built up.

The results suggest a fundamental difference in the convective life cycle between land and ocean. African storms evolve from convectively active systems with frequent lightning in their developing stages to more stratiform conditions as they dissipate. Over the Atlantic, the convective fraction remains essentially constant into the dissipating stages, and lightning occurrence peaks late in the life cycle. This behavior is consistent with differences in convective sustainability in land and ocean regions as proposed in previous studies.

The area expansion rate during the developing stages of convection is used to provide an estimate of the intensity of convection. Reasonable correlations are found between this index and the convective system lifetime, size, and depth.

1. Introduction

Deep convective systems and their associated ice cloud anvils dominate the rainfall and cloudiness over much of the Tropics. As well as their importance to the local climate, these systems may influence global cloud feedback through both direct radiative effects and their role in maintaining large-scale circulations and moisture distributions. However, the response of these systems to a climate perturbation is highly uncertain, with numerous, sometimes contradictory, potential mechanisms proposed in recent years (Ramanathan and Collins 1991; Chou and Neelin 1999; Lindzen et al. 2001; Hartmann and Larson 2002; Del Genio et al. 2005). Moreover, the processes involved in the development of these systems are often poorly represented by simplified parameterizations or are completely missing in climate models. Most GCMs are formulated strictly in terms of cumulus mass fluxes, with no ability to predict mesoscale structure or convective intensity, which change as convective systems evolve and differ markedly between land and ocean (Zipser and Lutz 1994; Zipser et al. 2006).

Quantifying the characteristics of convective systems as they evolve over their life cycles would provide a useful validation standard, as well as perhaps some developmental insights for GCM cumulus parameterization. Tracking of convective systems in geostationary satellite images provides a means to study this evolution. Early studies manually tracked systems during the Global Atmospheric Research Program (GARP) Atlantic Tropical Experiment (GATE) field campaign, providing insights into the nature of the westward

Corresponding author address: J. M. Futyan, Institute for Space Studies, Columbia University, 2880 Broadway, New York, NY 10025.
E-mail: jfutyan@giss.nasa.gov

DOI: 10.1175/JCLI4297.1

Unauthenticated | Downloaded 03/24/25 02:03 PM UTC

propagating squall lines that form over elevated African terrain (Aspliden et al. 1976; Desbois et al. 1988), and their relationship to synoptic-scale easterly wave disturbances (Payne and McGarry 1977). More comprehensive studies became possible following the pioneering demonstration of objective automated tracking by Williams and Houze (1987). Hodges and Thorncroft (1997) and Mathon and Laurent (2001) confirmed the strong diurnal modulation and orographic forcing of convection over Africa using multiyear geostationary infrared (IR) satellite observations and further emphasized the importance of the large organized systems, which provide around 90% of the rainfall in the Sahel region (Mathon et al. 2002). Organized systems also dominate in the Pacific warm pool region, where they merge into "super clusters," which are modulated by the intraseasonal oscillation (Mapes 1993; Mapes and Houze 1993; Chen et al. 1996). Building on these studies, Machado et al. (1998) examined the evolution of system size and vertical extent by compositing tracked clusters according to their life cycle duration, while Sherwood and Wahrlich (1999) examined the evolution of the atmospheric state by compositing sounding data into life cycle stages determined from the fractional area of very cold cloud tops in the western tropical Pacific.

Observations from the Tropical Rainfall Measuring Mission (TRMM) precipitation radar (PR), Microwave Imager (TMI), and Lightning Imager Sensor (LIS) have provided insights into the regional and interannual variability of the properties of convection. Schumacher and Houze (2003a) analyzed PR data and highlighted large regional differences in the stratiform rain fraction, with maximum values occurring in the oceanic convergence zones, while Boccippio et al. (2000) used LIS data to show that lightning occurrence and flash rate are strongly concentrated over land. Nesbitt et al. (2000), Toracinta et al. (2002), and Cecil et al. (2005) combined TMI and PR observations to create a comprehensive database of convective events, which they have used to further investigate the regional variability in the occurrence and properties of intense convection. Petersen and Rutledge (2001) also used PR and LIS data to compare the vertical structure of convection between regions, demonstrating that infrequent lightning and rapid decay in radar reflectivity above the melting level are characteristic of remote interior ocean regions.

Convection in Africa is some of the most intense on the earth, with significant ice scattering aloft and frequent lightning (Zipser et al. 2006). The GATE (oceanic) and Convection Profonde Tropicale (COPT81: continental) field campaigns provided radar observations of squall lines in both the African and Atlantic regions (e.g., Houze and Betts 1981; Houze and Rappaport 1984; Chong et al. 1987; Roux 1988). However, differences in instrumentation meant that only qualitative comparisons between land and ocean systems were possible. Using a climatology of TRMM radar observations Geerts and Dejene (2005) found that African storms are deeper and less stratiform in nature than Amazonian storms. Schumacher and Houze (2006) found similar differences between African systems and those over the neighboring Atlantic Ocean, which they attributed to differences in convective sustainability between land and ocean (Yuter and Houze 1998).

Combining IR observations of the cloud field with radar observations provides valuable additional information. Houze and Rappaport (1984) jointly analyzed geostationary IR satellite imagery and 3D ship radar data to characterize the life cycle of a squall line off the coast of Africa. TRMM provides only a single snapshot of each convective system, preventing study of the evolution of individual convective events. However, by matching the TRMM observations with life cycle information from a database of tracked storms based on geostationary satellite observations, it is possible to build up a composite picture of the evolution of the vertical structure of convection. This study describes a methodology by which this can be achieved and uses this technique to reveal some interesting differences in the convective vertical structure and intensity evolution between the African and Atlantic regions.

2. Data and methodology

Four months (June–September 2005) of broadband thermal flux images from *Meteosat-8* are used to detect and track convective systems in the Atlantic (10°S–20°N, 50°W–20°E, ocean only) and African (20°S–30°N, 20°W–50°E, land only) regions. As data from the Geostationary Earth Radiation Budget (GERB) experiment were not available at the time of writing, GERB-like data, produced using a narrowband to broadband conversion of the Spinning Enhanced Visible and Infrared Imager (SEVIRI) data, are used here. The estimation of broadband quantities, rather than direct use of the narrowband radiances, provides quantities more directly comparable to standard model outputs.

Estimates of the broadband radiance are produced from SEVIRI via a multichannel regression (Clerbaux and Dewitte 1999). Angular dependency models from Clouds and the Earth's Radiant Energy System (CERES: Loeb et al. 2003) are used for shortwave radiance to flux conversion, and theoretical limb darken-

Unauthenticated | Downloaded 03/24/25 02:03 PM UTC

ing values combined with a regression on the SEVIRI channels are used in the longwave (Clerbaux et al. 2003). This procedure has previously been used by Futyan et al. (2005) to estimate cloud forcing over the *Meteosat-8* region. The data have a spatial resolution of ≃45 km at nadir and a 15-min temporal resolution, although an hourly subset is used here for system tracking. The use of reduced-resolution data (hourly, ≃45 km) rather than full-resolution imagery (15 min, ≃15 km) limits the minimum size of the systems that can be tracked. However, previous studies have shown that reduced-resolution data are adequate for the tracking of larger, mesoscale features (Hodges and Thorncroft 1997; Machado et al. 1998). The averaging, rather than subsampling, of the data also smoothes out local minima in brightness temperature.

The TRMM 3B42 merged infrared and microwave satellite rainfall product (Huffman et al. 1997) is used to provide a 3-hourly estimate of the system-average rain rates and rain area fraction. Data from the TRMM PR and LIS are also matched to the systems tracked in the geostationary flux images, allowing a composite picture of the system evolution to be built up. The PR (Kozu et al. 2001) is a 14-GHz radar with a swath width of 240 km and a horizontal resolution at the ground of ≃5 km (since the orbit boost in August 2001). The LIS (Christian 1999) is a staring imager designed to locate and detect lightning with a 90% efficiency at a resolution of ≃4 km over a 600-km swath. The 35° inclination orbit of the TRMM satellite provides coverage of regions from approximately 35°S–35°N, with observation time precessing through the diurnal cycle on successive orbits.

The near-surface rain rate, rain type (convective versus stratiform) identification, and reflectivity profiles are extracted from the PR version 6 2A25 data. Rain type is determined based on the horizontal and vertical structure of the radar echoes (Awaka et al. 1997). Rain rates are estimated from the attenuation-corrected radar reflectivities using a Bayesian approach (Iguchi et al. 2000). Lightning occurrence and flash rates are determined from the LIS version 4.1 dataset.

Due to the limited swath width (particularly for PR) only a portion of each system is sampled. Grazing samples are rejected; for inclusion, data must be available for at least 30% of the system area or for at least 10 GERB footprints within the system. For the 4 months of data considered here, this provides about 2000 matched observations for PR (982 over land and 459 over ocean and the remainder over coastal regions) and about 3400 for LIS, from a total of nearly 8000 tracked systems. For a system to be defined as land or ocean based all of the footprints within it must be of that surface type. Any system where any part of the anvil extends over the West African coast is defined as coastal.

a. Detecting and tracking convective systems

Thresholding on the infrared brightness temperature is commonly used to identify "convective regions" within a satellite field of view (Williams and Houze 1987; Mapes 1993; Chen et al. 1996; Hodges and Thorncroft 1997; Boer and Ramanathan 1997; Machado et al. 1998; Mathon and Laurent 2001). While there is little correspondence between the IR brightness temperature and the fraction of convective rainfall (Yuter and Houze 1998), areas of strongly depressed IR temperature do provide a tracer of the cold, predominantly precipitating, cloud associated with convection in tropical regions.

As we wish to track the systems through their entire life cycle and to include as much of the anvil cloud associated with the convective activity as possible, we use a detection algorithm based on the multiple threshold "detect and spread" approach proposed by Boer and Ramanathan (1997). An initial threshold (165 W m^{-2} or ≃232 K) is applied to the flux image to define cold system cores. This is warmer than the 208–220 K values typically used to identify a precipitating system core but is found to perform better than colder values for the coarser-resolution GERB-like data (compared to IR window channel data typically used in previous studies).

Each contiguous region below this threshold is identified as a separate system core. These cores are then expanded outward until a second, warmer, threshold is reached (200 W m^{-2} or ≃244 K). If multiple system cores lie within a single continuous region of warmer cloud, the warmer "anvil" cloud is shared between the systems as they are spread outward. Continuous regions of cloud colder than 200 W m^{-2}, which do not contain any pixels colder than 165 W m^{-2}, are identified as new systems without a cold core. This process is repeated until all systems have been grown to the warmest threshold value, which is 235 W m^{-2} or ≃254 K in this case.

If a single threshold value is used to identify convective systems, there is a trade-off between the need to define distinct systems (which is best achieved at a cold threshold value) and the desire to include as much of the associated cloud cover as possible (which requires a warm threshold). The detect and spread approach avoids this problem by using a cold threshold to determine the identity of the systems but a warmer outer limit to determine their spatial extent. The approach also allows systems to be tracked through stages of de-

Unauthenticated | Downloaded 03/24/25 02:03 PM UTC

velopment where no cold core is present, hence providing a more complete picture of the spatial and temporal structure than tracking with a single threshold.

The precise choice of threshold values is somewhat arbitrary. Appropriate values depend on the spatial resolution of the data and on the wavelength used. For deep, optically thick clouds, the broadband brightness temperature (derived from the flux using the Stefan–Boltzmann relation) is comparable to the window channel value. For optically thinner clouds the broadband temperature estimate is lower than the window channel value. Visual comparison with spatially averaged IR window data suggests that the broadband thresholds used here (232, 244, and 254 K) are roughly comparable to window channel values of 240, 260, and 273 K. These values lie within the range used in the studies listed above and sensitivity tests (see section 5) indicate that our results do not depend strongly on the precise values chosen.

Systems are tracked throughout their life cycle using hourly flux data. Where data are missing at the nominal time, the data from the closest available GERB time step (within ±30 min) are used instead. Where no replacement file is available, the time step is flagged as missing. If only one time step is missing, the system properties at that time are filled with a missing data flag and the tracking continues at the next time step. If more than one time step is missing, all existing tracks are terminated and a new set of tracks initiated after the data gap.

Tracking is performed iteratively using a maximum area overlap approach, as proposed by Williams and Houze (1987). Machado et al. (1998) have demonstrated that this simple approach performs comparably to more complex tracking algorithms. For each system identified in the new image, if the cold core of that system overlaps with more than 50% of the cold core of a system in the previous image, they are identified as the same system. If not or for new systems without cold cores, overlap is calculated at the warmer thresholds. Where two systems merge, the larger, deeper system is considered to continue and the smaller part to terminate. Similarly, where a system splits, the larger fragment is considered as the continuation. For the hourly data used here, our overlap criterion can accommodate both the rapidly moving ($\simeq$60–80 km h^{-1}: Machado et al. 1998; Mathon and Laurent 2001) squall lines (provided these are larger than a few GERB footprints) and the slower nonsquall clusters found in this region (Houze and Betts 1981).

All systems present in three or more consecutive images that reach a minimum brightness temperature of 238 K (−35°C) at some point during their life cycle are tracked. Systems are subsequently divided into three categories based on the maximum size and minimum brightness temperature ($T_{\min}$) reached during the life cycle. "Large deep" systems (which we focus on here) reach $T_{\min} < 220$ K and must achieve a maximum effective radius (defined as $R_e = \sqrt{A/\pi}$) > 300 km at the warmest threshold. Systems that reach $T_{\min} < 220$ K but remain smaller than 300 km in radius are identified as "small deep," while systems of any size with $T_{\min}$ between 220 and 238 K are described as "intermediate" systems. These divisions are marked on the overall distribution of system sizes and temperatures shown in Fig. 3.

b. Defining life cycle stage

The evolution of the system radius and minimum brightness temperature is used to define the life cycle stage. The expected evolution of a convective system begins with vertical growth of a convective core, followed by expansion of the anvil and subsequent dissipation. For each tracked system a sixth-order polynomial (lower orders are used for systems with lifetimes of less than six hours) is fitted to the radius and temperature data to determine the time where the minimum temperature is first reached and the time of maximum spatial extent. Before the minimum in brightness temperature, the system is growing vertically and is considered to be "developing." The subsequent period of horizontal growth is considered to be the "mature" stage, and the system is considered to be dissipating after the maximum radius is reached. The developing and dissipating stages are further divided into "cold" and "warm" portions based on the minimum brightness temperature. Figure 1 shows the temperature and radius data and the resulting life cycle stage classification for an example of an African land-based storm.

This definition of life cycle stage provides a framework to compare the evolution of African convective systems with oceanic systems in the Atlantic intertropical convergence zone (ITCZ). By matching the tracked systems to TRMM overpasses, TRMM snapshots can be evaluated in the context of the system evolution. Plotting results as a function of life cycle stage rather than time since formation allows data for systems with a wide range of lifetimes to be combined in a meaningful way. Since the life cycle definition is based on tendencies of the system size and temperature, life stages can be defined even when the entire life cycle is not observed (e.g., where the system forms in a split and, hence, no developing stage is observed). This is particularly valuable for producing composites from the relatively sparse TRMM datasets.

Approximately 15% of the systems tracked show

Unauthenticated | Downloaded 03/24/25 02:03 PM UTC

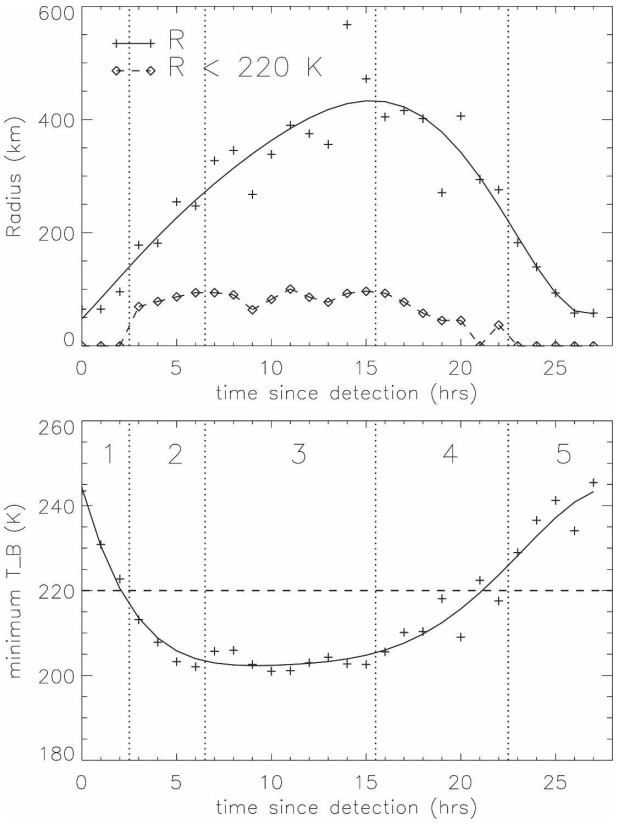

FIG. 1. Example of system radius (R) and brightness temperature (T_B) evolution for an African land convective system and the corresponding life cycle stage classification. Numbers in lower panel give the life cycle stage—1: warm developing, 2: cold developing, 3: mature, 4: cold dissipating, 5: warm dissipating.

more complex evolution than this simple picture suggests, with multiple maxima in radius or minima in brightness temperature. Inspection of the behavior for a subset of these cases suggests that this apparent regeneration can result from real strengthening of convection, from mergers of dissipating systems with nearby developing cells, or, on occasion, from failures of the system identification and tracking code. Over land, regeneration frequently occurs around local noon in response to the diurnal forcing of surface heating. However, nocturnal regeneration is also observed in some cases.

The regenerating systems occur throughout the region considered and account for about 45% of the total cold cloud cover and around 30% of the total rainfall. While these systems clearly play an important role in the local climate, they are excluded from the following analysis to ensure robust definition of the life cycle stages. Regenerating systems are slightly larger and longer lived on average than nonregenerating systems, but their properties (lifetime, size, depth, and rain rates) lie within the same range of values as are observed for nonregenerating systems, suggesting that the "well behaved" subset considered here is representative of the wider population.

The life cycle classification also fails in approximately a further 10% of cases, either because the maximum size precedes the minimum brightness temperature (<2% of systems and <2% of cold cloud cover) or because the evolution of the brightness temperature and radius is ambiguous. These latter cases are mainly short-lived fragments and contribute little to the total cloud cover or rainfall.

3. System properties and evolution from geostationary data

Figure 2 shows the spatial distribution of convective activity over the African and Atlantic region. The regions of peak genesis frequency over Africa correspond well with regions of higher elevation (not shown) as found by Hodges and Thorncroft (1997). Large deep systems dominate over central to eastern Africa and close to the West African coast. A smaller fraction of systems meet the criteria for large deep systems over the Atlantic with both the system size and, most clearly, cloud height decreasing over the ocean to the west of the African region.

Distributions of the system lifetime (for the subset of systems tracked from genesis to dissipation), the peak system size reached ($R_{\max}$), and the minimum brightness temperature reached ($T_{\min}$) are shown in Fig. 3. The vertical lines in Fig. 3 show the separation of deep versus intermediate ($T_{\min}$ </> 220 K) and large and small ($R_{\max}$ >/< 300 km) systems. As found in previous studies, small short-lived systems dominate the population over both land and ocean, but the less frequent larger and longer-lived systems provide most of the cloud cover and rainfall (Williams and Houze 1987; Mapes and Houze 1993; Machado et al. 1998; Roca and Ramanathan 2000; Mathon and Laurent 2001; Wilcox and Ramanathan 2001). The large deep systems considered here contribute roughly 80% of the total area with cloud tops colder than 254 K. Note that our size definition includes much of the warmer, nonprecipitating anvil cloud and is thus larger than many previous estimates. The cold-core ($T < 232$ K) area is much smaller, exceeding 300 km for less than 10% of the population.

There is a clear difference in the distribution of cloud-top heights between the African and Atlantic regions, with a much larger population of systems with $T_{\min} > 220$ K over the Atlantic. These systems are still deep, with cloud tops at around 10 km, consistent with GATE divergence and heating rate profiles (Thompson

Unauthenticated | Downloaded 03/24/25 02:03 PM UTC

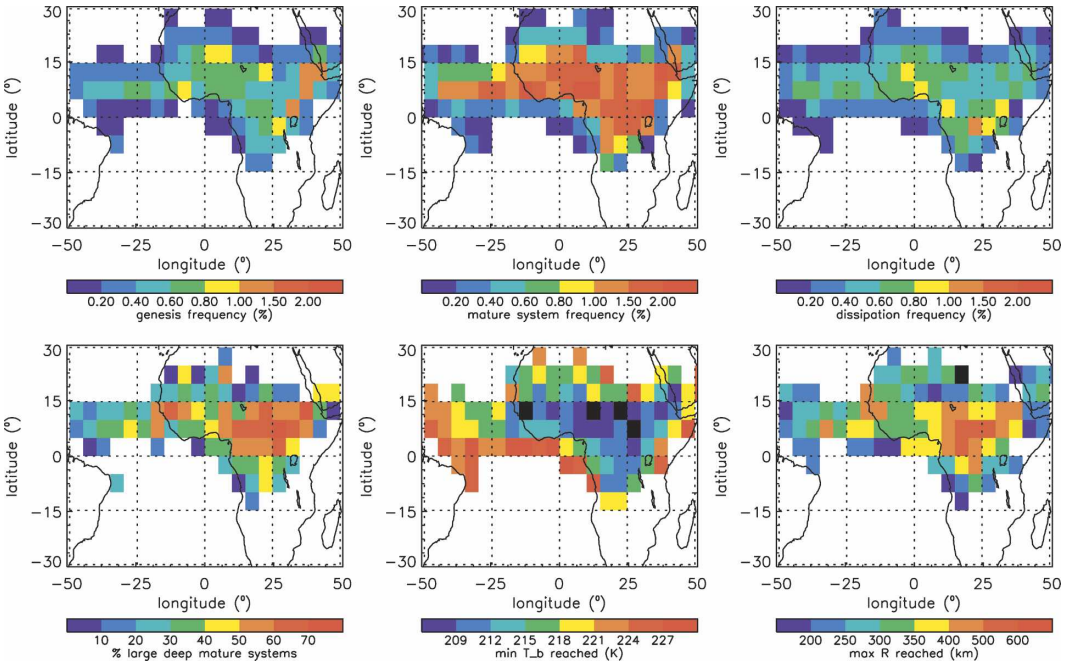

FIG. 2. (top left) Maps showing locations of system genesis, (top middle) maturity, and (top right) dissipation frequency. Values indicate the percentage of systems occurring within each 5° grid box. Also shown are the spatial variability of (bottom left) the relative frequency of large deep systems, (bottom middle) the average lifetime minimum brightness temperature, and (bottom right) the average maximum system radius reached for each grid box.

et al. 1979). However, they are not as vertically developed as many land-based storms, which extend close to the tropopause height [based on the regional and seasonal mean National Centers for Environmental Prediction (NCEP; Kalnay et al. 1996) reanalysis temperature profile, $T_{\min} \simeq 200$ K corresponds roughly to a height of 16 km]. Distributions of size and lifetime are similar for the two regions, although land-based systems tend to be slightly larger and lifetimes greater than 24 h occur slightly more frequently over the ocean, a result also seen elsewhere in the Tropics (Williams and Houze 1987). As found in many previous studies (e.g., Houze and Cheng 1977; Martin and Schreiner 1981; Chen et al. 1996; Machado et al. 1998; Mathon and Laurent 2001), larger deeper systems tend to be longer lived. Almost all intermediate systems live for less than

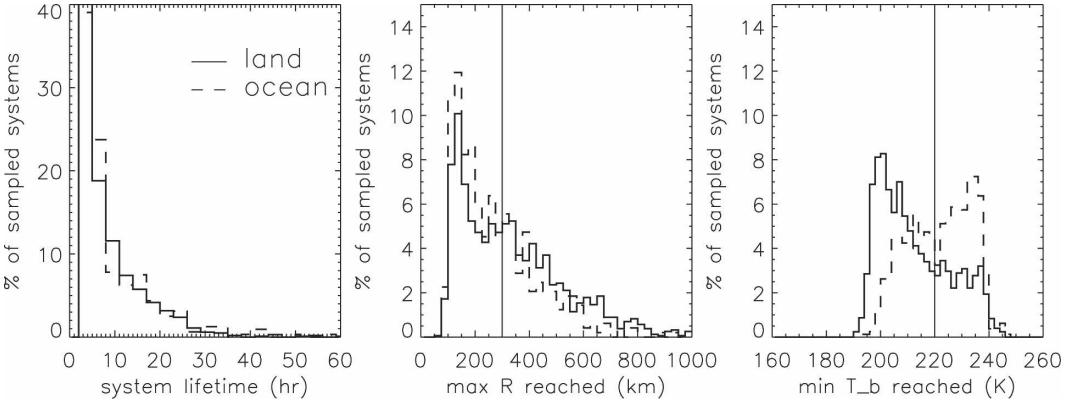

FIG. 3. Histograms of (left) system lifetime, (middle) peak equivalent radius reached $R_{\max}$, and (right) minimum brightness temperature reached $T_{\min}$. The vertical lines show the separation of the deep vs intermediate ($T_{\min}$ </> 220 K) and large and small ($R_{\max}$ >/< 300 km) systems defined in section 2a.

Unauthenticated | Downloaded 03/24/25 02:03 PM UTC

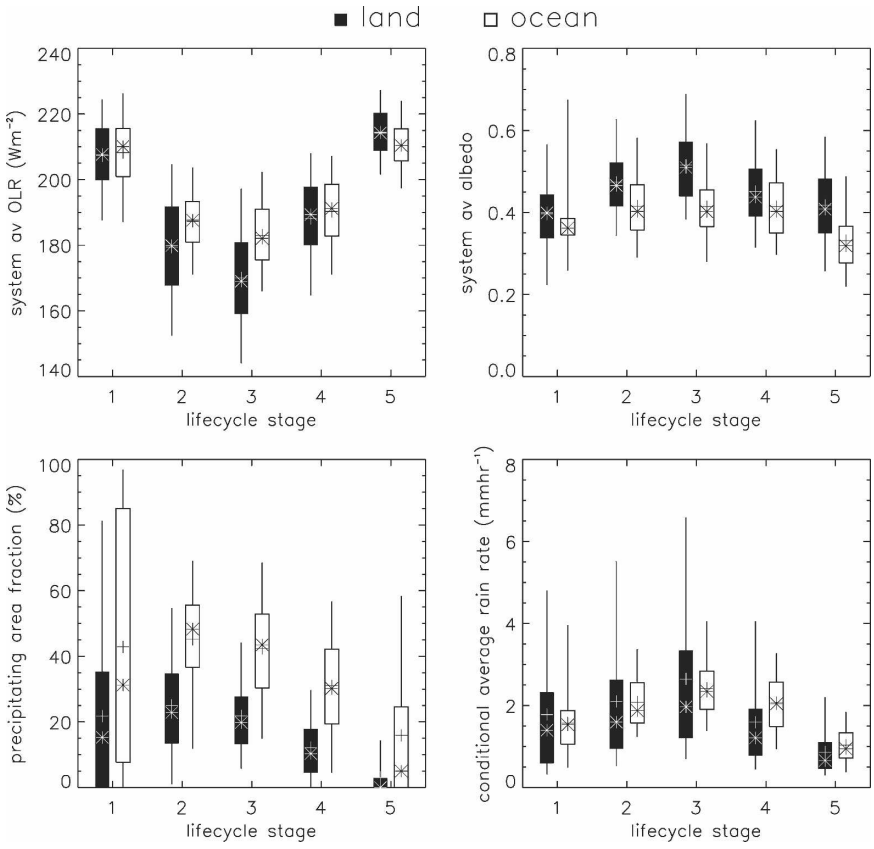

FIG. 4. Comparison of the evolution of radiative [(top left) OLR and (top right) albedo] and precipitation properties [(bottom left) precipitating area fraction and (bottom right) conditional average rain rate] for large deep Atlantic (ocean) and African (land) convective systems. The box covers 25th–75th percentile and the whisker 5th–95th. The + indicates the mean and * denotes the median value. Based on GERB-like and TRMM 3B42 data. Life cycle stage numbers are defined in Fig. 1.

12 h, with a typical lifetime of around 6 h over both land and ocean. Deeper systems last longer, particularly over ocean, with median lifetimes of 11 (17) h for small deep land (ocean) systems and 21 (27) h for large deep systems.

Figure 4 compares the evolution of the radiative [system-averaged GERB-like outgoing longwave radiation (OLR) and albedo] and precipitation (TRMM 3B42 precipitating area fraction and conditional average rain rate) properties for large deep African land and Atlantic ITCZ systems. Properties are calculated for the entire system area. Even for this large, vertically developed subset of the systems, land-based systems are deeper and brighter than oceanic systems throughout the life cycle. However, Atlantic systems have higher precipitating area fractions. Conditional (averaged only over the precipitating portion of the system) rain rates are similar for land and ocean, although oceanic systems remain more heavily precipitating in the dissipating stages. These results are consistent with the presence of more extensive stratiform rain areas over the ocean (Schumacher and Houze 2003a, 2006). The less pronounced decay in the later stages of the life cycle observed over ocean is explored further in sections 5 and 7.

Similar results are found for small deep and intermediate systems (not shown). Ocean systems have greater precipitating fractions and lower mean albedo than land systems for all three system types, while land systems have smaller mean OLR than ocean systems for the two deep classes but comparable values to ocean systems for the intermediate class. Over both regions, large systems reach lower $T_{\min}$ than smaller systems. System average OLR is, however, only slightly less for the large systems, and albedos are similar (slightly lower for large deep systems than for smaller ones over land). This suggests that the larger systems contain more extensive regions of optically thinner cloud. This

Unauthenticated | Downloaded 03/24/25 02:03 PM UTC

appears to be true even in the early stages of development (stage 1) over land where, despite similar distributions of T_{min}, mean OLR is higher and albedo lower for systems that go on to reach large sizes. Precipitating area fraction is comparable for small and large deep systems over land but significantly lower for intermediate systems. Over the Atlantic, the precipitating fraction is highest for small deep systems, though the largest rain areas are found in large deep systems.

4. Vertical structure of mature African and Atlantic systems

Following Yuter and Houze (1995), we present a statistical summary of the radar observations in the form of a 2D frequency distribution or contoured frequency by altitude diagram (CFAD). Figure 5 shows the accumulated (over all observed storms) distribution of radar reflectivity for mature (life cycle stage 3) large deep systems over Africa and the Atlantic. Also shown are the median and quartile reflectivity profiles for the convective and stratiform regions of these storms. Shallow convective profiles are not included in either the convective or stratiform distributions, although the effect of their inclusion is discussed in section 5 below. Results are based on over 100 000 (40 000) PR profiles from 110 (34) storms for the African (Atlantic) regions.

As found by Schumacher and Houze (2006), convection is much deeper and, on average, more intense (higher peak reflectivity) over Africa than over the Atlantic. Comparing the frequency distribution with the two sets of profiles also confirms that stratiform rainfall is more prevalent over the ocean where it produces a strong brightband signature at ≃5 km altitude.

The reflectivity in the stratiform portion of the systems decreases below the melting layer over the African region. Hirose and Nakamura (2004) find that such downward-decreasing profiles are common over interior landmasses in summer and suggest they may result from reevaporation of rainfall in dry subcloud air. Such reevaporation may contribute to the lower mean storm average stratiform rain rate (1.1 mm h^{-1} over land, 2.1 mm h^{-1} over ocean) and higher virga fraction observed here for African systems. Storm-average convective rain rates for large deep systems over the Atlantic (10.6 mm h^{-1}) are larger than those over the land (7.8 mm h^{-1}). Schumacher and Houze (2006) found lower mean convective rain rates over the east Atlantic than for West Africa. This difference results from differences in the algorithm used to convert the measured radar reflectivity (Z) to rain rate (R). Schumacher and Houze (2006) applied a fixed Z–R relationship to version 5 PR reflectivity data, while in the version 6 PR data used here the Z–R relationship is adjusted to be consistent with the droplet size distribution implied by the attenuation correction (Iguchi et al. 2000). Further investigation is required to determine whether the larger oceanic rain rates implied by the version 6 algorithm are realistic; however, this is beyond the scope of this paper. Furthermore, we find that our subsequent results are qualitatively robust to the choice of Z–R conversion algorithm.

The average precipitating area fraction (nonzero surface rain) is higher over ocean (23%) than land (12%) for large deep storms, owing primarily to more extensive stratiform rain areas (18% of total system area on average over ocean, only ≃9% over land). These values are significantly lower than those derived from the 3B42 (combined infrared and microwave) product (see Fig. 4). Subsampling the 3B42 results only where PR data are available and gridding the PR data to match the 0.25° resolution of 3B42 suggests that this is primarily due to the difference in resolution (coarser resolution data give lower rain rates over a larger area), but also reflects a bias between the two datasets, with 3B42 overestimating the rain area, particularly over ocean. In any case, both data products imply substantially higher precipitating area fractions over ocean.

Consistent with the frequent occurrence of large reflectivities in the mixed phase region of the cloud (Fig. 5), lightning is observed in over 80% of the mature large deep African systems observed by LIS. In contrast, only 14% of the mature large deep systems observed over the Atlantic contain lightning. Flash rates are also much lower for the oceanic systems (see also Fig. 8 in section 5). This contrast in the frequency of lightning between continental and oceanic convection is well known (Orville and Henderson 1986; Zipser 1994; Christian and Latham 1998). The higher frequency of occurrence of lightning over land is believed to be primarily due to higher updraft velocities in continental convection lofting large ice particles and supercooled water into the mixed phase region (LeMone and Zipser 1980; Rutledge et al. 1992; Lucas et al. 1994; Williams and Stanfill 2002). However, differences in aerosol concentrations between land and ocean may also play a role through the suppression of warm rain processes in continental regions (Rosenfeld and Lensky 1998; McCollum et al. 2000; Sherwood et al. 2006).

The distributions of convective profiles for large deep systems within which lightning was observed (Fig. 6) are almost identical to the overall distribution (Fig. 5) over land and only slightly deeper and stronger over ocean. However, when only profiles collocated with an observed lighting flash are retained, we find deeper profiles over both land and ocean with smaller differ-

Unauthenticated | Downloaded 03/24/25 02:03 PM UTC

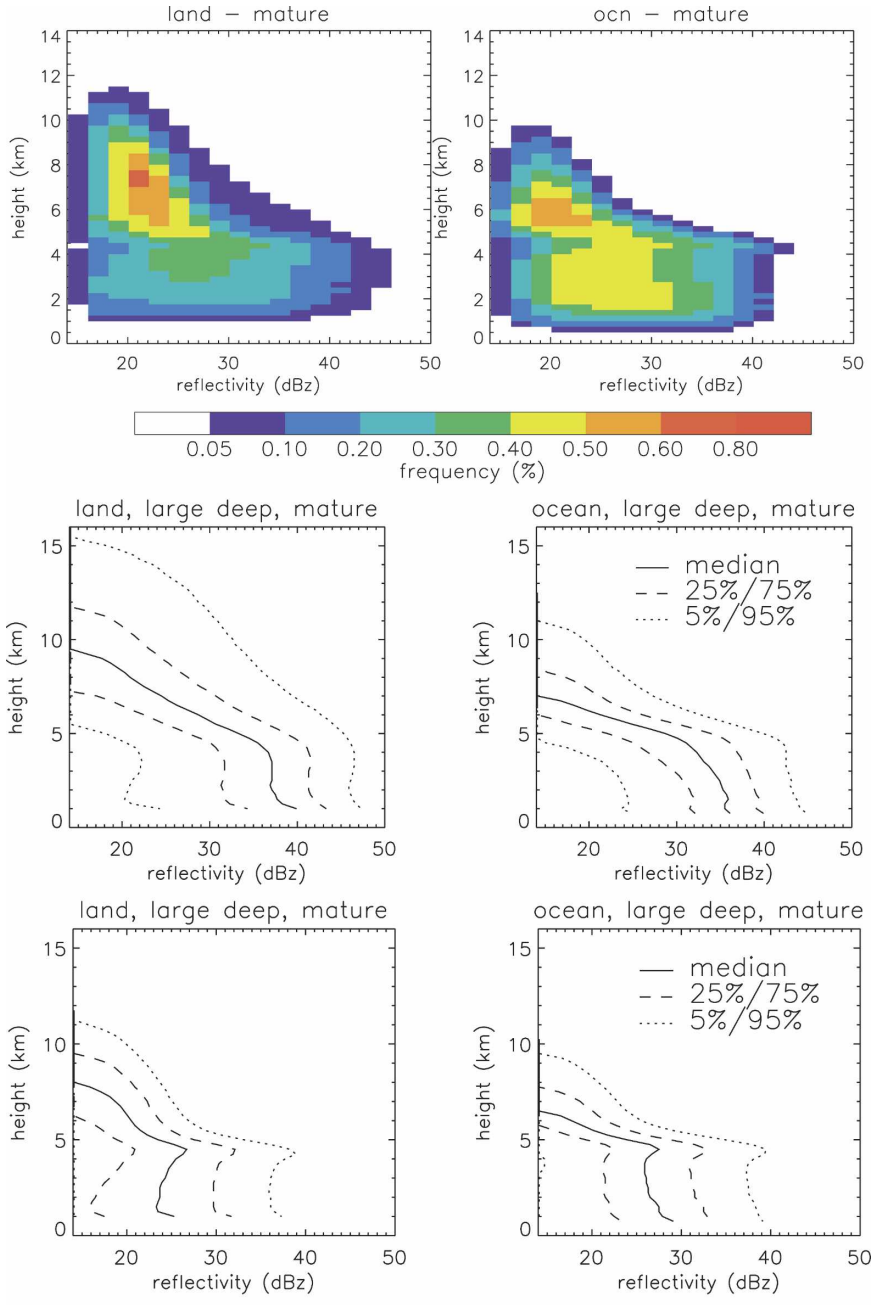

FIG. 5. Frequency distribution of (top) radar reflectivity, and median and quartile profiles for (middle) convective and (bottom) stratiform regions of mature African and Atlantic convective systems. Reflectivity values below the sensitivity of the PR radar have been filled with the minimum detectable echo value of 14 dBZ. This preserves the true median reflectivity at each level and prevents the profile from being biased toward a deeper subset of profiles higher in the atmosphere. Values flagged as missing due to ground clutter, etc., have not been replaced.

ences between the two. These profiles represent the deepest 25% of land profiles but lie outside of the 95th percentile of the overall distribution over ocean.

Due to the smaller system sizes and shorter lifetimes, relatively few PR–GERB matched observations of small deep and intermediate systems are available during the 4-month period considered (≃20 overpasses of mature systems for the African region and <10 over the

Unauthenticated | Downloaded 03/24/25 02:03 PM UTC

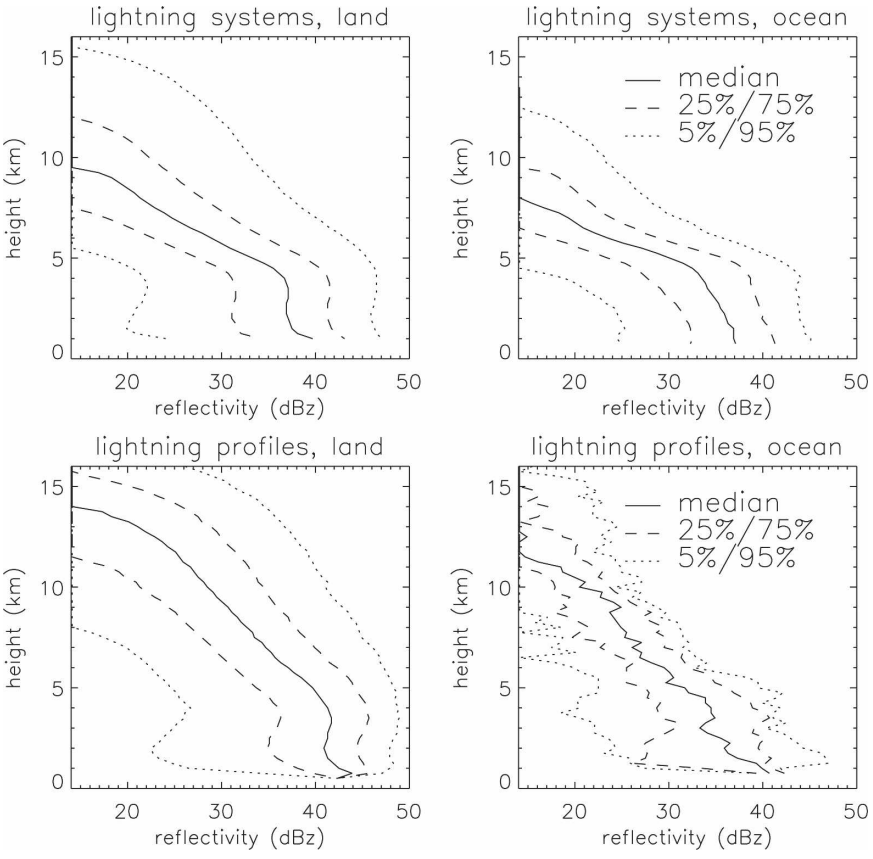

FIG. 6. (top) Median and quartile convective profiles for mature African and Atlantic convective systems with lightning observations and (bottom) profiles from PR footprints collocated with observed lightning flashes. As in Fig. 5, reflectivity values below the sensitivity of the PR radar have been filled with the minimum detectable echo value of 14 dB*Z*.

Atlantic). For the small deep systems that we do observe, the reflectivity distributions (Fig. 7) are similar to those for the larger deep systems (Fig. 5), although the stratiform signal (brightband spike at the melting layer and rapid decay above it) is weaker, particularly over land. This is primarily due to the smaller fractional coverage by stratiform rain [6% of the total system area for small deep land systems (4% if only regions with nonzero surface rain rate are included)]. However, separation of profiles for convective and stratiform regions (not shown) also shows that much of the stratiform rain area within small deep systems exhibits a rather weak echo with little or no surface rain and no discernable brightband signal. These regions are flagged as stratiform based on the horizontal pattern of radar echoes (Awaka et al. 1997) but are often similar to the "other" or anvil only echoes found to occur frequently over West Africa by Schumacher and Houze (2006).

These weak stratiform and anvil profiles are also associated with the relatively gradual decrease in reflectivity with height (compared to oceanic systems) above the melting layer seen in the stratiform profiles for large deep land systems (Fig. 5). Profiles of this type also occur over ocean but are a much smaller fraction of the total "rain area." Areas with significant radar echo from precipitation-sized particles aloft but little or no surface rain over Africa may be partially to blame for the discrepancy between passive microwave- and infrared-based rain estimates and surface rain gauge data (McCollum et al. 2000).

Over both land and ocean, distributions of convective profiles for small deep systems (not shown) are very similar to those for large deep systems (Fig. 5), suggesting that the horizontal extent of the system is not simply controlled by the depth of the convective cells within it. Somewhat shallower and less intense (lower peak reflectivity) convection is observed for the intermediate systems. Roughly 70% of small deep land systems have lightning during their mature stage (almost 100% do during the developing stage), while only about 40% of intermediate systems do. Lightning occurrence is comparable for small deep and large deep

Unauthenticated | Downloaded 03/24/25 02:03 PM UTC

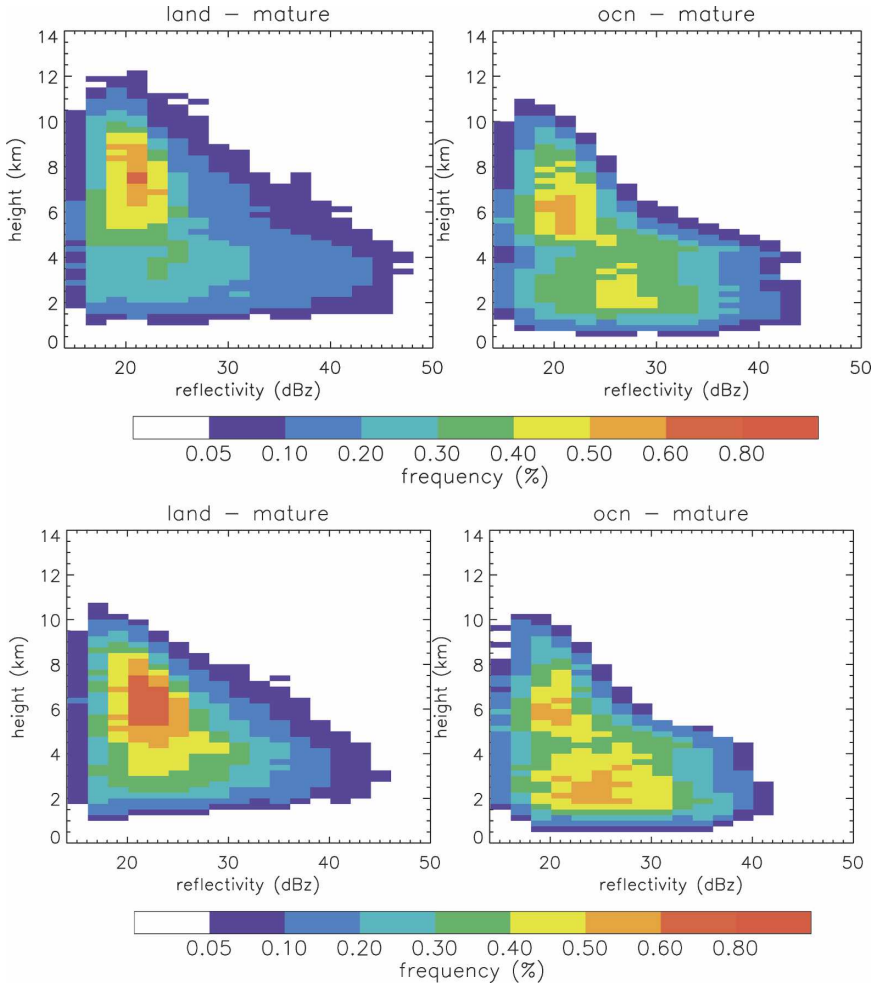

FIG. 7. Frequency distribution of radar reflectivity for mature (top) small deep and (bottom) intermediate systems for the African and Atlantic regions.

systems over the Atlantic, but none of the intermediate ocean systems were observed to produce lightning.

5. Evolution of African and Atlantic systems

Due to the small sample size for matched PR observations of small deep and intermediate systems, results for the rain type and system vertical structure evolution are only presented for large deep systems. The warm and cold developing stages have also been combined to provide a reasonable sample size (>20 systems) in each bin. Comparison of the system properties determined from only the subset of systems sampled by the PR (not shown) with the results for the overall populations shown in Fig. 4 confirms that this subset is representative of the wider population.

Figure 8 shows the evolution of the convective and stratiform rain volume fractions for both land and ocean systems. Over land, convective rainfall dominates the developing and mature stages of the system evolution, and stratiform rain becomes more important as the systems dissipate. Over ocean, the life cycle is less well defined, with the stratiform rain fraction essentially constant throughout the life cycle. The range of values for each life cycle stage in these plots comes both from differences between systems and from differences in the portion of the system sampled in each case. The strength and depth of oceanic convection also varies little over the life cycle (although weaker, shallow profiles are observed in the final dissipating stage), while over land the deepest, most intense convection is observed for mature systems.

Warm rain profiles (defined here as profiles with echo top height more than 1 km below the climatological melting layer) have been excluded in generating these plots. Over land, the contribution to the total

Unauthenticated | Downloaded 03/24/25 02:03 PM UTC

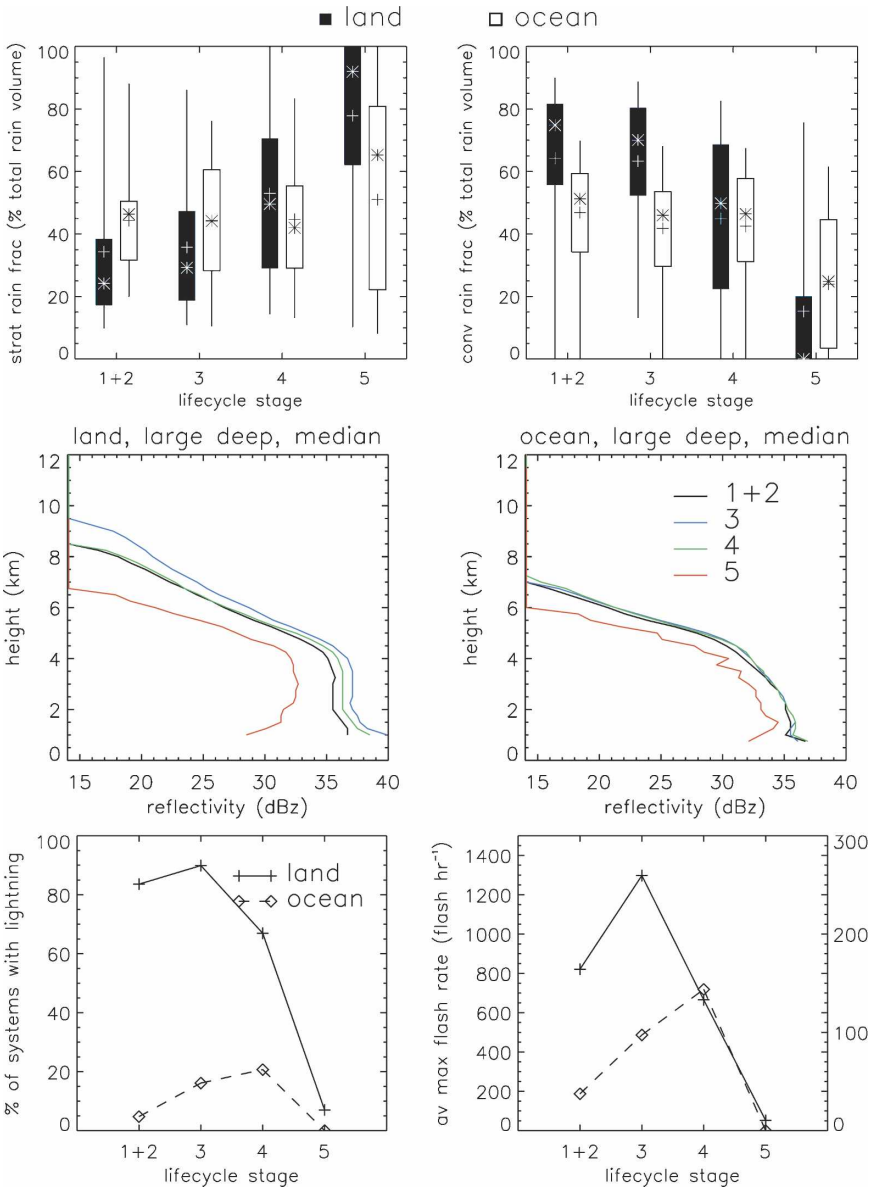

FIG. 8. (top) Convective and stratiform rain fractions (% of measured rain volume = rain rate × rain area flagged as convective, etc.) as a function of life cycle stage for large deep land and ocean convective systems. (center) Median convective profiles as a function of life cycle stage for large deep land and ocean convective systems. (bottom) Lightning occurrence (% of sampled systems) and mean storm maximum flash rate as a function of life cycle stage for large deep land (solid line) and ocean (dashed line) systems. Flash rates for ocean systems have been multiplied by a factor of 5 to show the variation over the life cycle, the appropriate scale is shown at the right-hand side of the plot.

rainfall from warm rain is negligible for deep systems, but 5%–10% of the total precipitation over the Atlantic comes from warm rain processes, even for large deep systems. Schumacher and Houze (2003b) argue that almost all of the warm rain identified by TRMM is convective in origin. If we assume that this is indeed the case and include warm rain in the convective rain fraction, values over ocean increase from ≃45% to ≃60%. However, there is still no clear evolution in convective–stratiform partitioning over the life cycle. Inclusion of warm rain as convective also exaggerates the difference in the depth and intensity of the convective profiles between land and ocean.

Differences in system evolution between land and

Unauthenticated | Downloaded 03/24/25 02:03 PM UTC

ocean are also suggested in the plots of lightning occurrence and average peak flash rate in Fig. 8. Consistent with the PR data, lightning occurs most frequently in the convectively active developing and mature stages over land. Over ocean, however, the peak activity occurs during the cold dissipating stage, consistent with the continued occurrence of frequent convection after the peak size is reached. As systems for which any part of the anvil extended over the coast have been excluded from the oceanic population, the observed behavior is expected to be representative of that over open ocean.

It is important to ask to what extent we have successfully identified and tracked distinct convective systems in each of the two regions. The complex interacting nature of convection means that it is not always straightforward to determine where one system ends and the next begins. Here, systems are defined by infrared signatures of the cold cloud associated with convective activity; the resulting system boundaries will not in general be the same as those that would be identified using microwave or radar data, which emphasize the smaller regions with significant rainfall or ice scattering aloft (e.g., Nesbitt et al. 2000). Over oceanic regions in particular, convection tends to be gregarious, with many systems influencing the development of one another over a large region (Mapes 1993; Mapes and Houze 1993).

We approached the validation of our system identification and tracking in two complementary ways. First, we conducted sensitivity tests to explore whether the statistics of land − ocean differences depend strongly on the assumptions made. Relaxing the overlap requirement used in the tracking code to 30% (from 50%) produces a less than 1% change in the percentage of systems identified as large deep and small (4 h and 10 km) increases in the median lifetime and maximum size of these systems. Increasing the initial detection threshold value to 185 W m^{-2} (from 165 W m^{-2}) causes the mean stratiform rain fraction to change by less than 5% in all life cycle stages and the mature stage median depth of convection to change by less than 200 m. The use of harsher matching requirements (requiring a larger percentage of the cloud region to be sampled by PR) and the exclusion of systems that showed only limited evolution in temperature and size (where the life cycle stage classification might be more uncertain) also do not lead to any qualitative differences in behavior. The well-defined evolution of the radiative and precipitation properties seen in Fig. 4 for both the African and Atlantic regions also gives us confidence that, for the well-behaved subset of systems analyzed, we are indeed successfully tracking systems over their life cycle, at least in a statistical sense.

Next, we performed a visual inspection of a subset of 40 cases with radar data and confirmed that the life cycle stage is correctly assigned in the majority of cases. Regional clusters of cold cloud can be identified in the larger pattern of interacting systems, and these are generally picked out and tracked successfully by our scheme. In general we find that limitations in the ability of the automated detection and tracking to identify systems correctly lead either to high frequency noise, which is eliminated by fitting smooth curves to the time series prior to determining the life cycle stage, or, less frequently, to a step change in the identity of the system being tracked. Situations where this latter behavior results in a switch from a dissipating to a developing system will be excluded as regenerating, and the use of broad life cycle categories means that the correct classification is otherwise usually correctly assigned.

Overall, the differences in evolution presented here are therefore believed to be robust and to genuinely reflect a difference in how convective systems develop between the African and Atlantic regions. The consistent story told by both the PR and LIS observations also adds confidence in these results. Additional support for the occurrence of continued frequent convective activity late in the system evolution over the Atlantic region comes from the GATE squall-line case study described by Houze and Rappaport (1984), where comparable convective and stratiform rain amounts were observed late in the life cycle, after the cold cloud area started to decrease (see their Fig. 9).

6. Nature of propagating systems

Since systems are classified as land, coast, or ocean based on their location at the time of observation, systems that form over land and propagate out over the Atlantic region will be redefined as oceanic systems and may influence the composite evolution observed. Most systems reaching the West African coast dissipate, leaving decaying fragments to move out over the ocean. Roughly one-third of the Atlantic large deep systems either propagated out from Africa or split from a dissipating system in the coastal region.

To test whether systems of nonoceanic origin are influencing the composite oceanic life cycle, the analysis was repeated including only "local ocean" systems, those which form over the Atlantic (and do not split from a coastal system) and remain there for their entire life cycle. The exclusion of nonlocal systems was found to have little impact. In fact, the two populations (local and nonlocal ocean) have remarkably similar properties and evolve in a similar manner once over open ocean (Fig. 9). The width of the coastal exclusion region depends on the size of the system, so small developing

Unauthenticated | Downloaded 03/24/25 02:03 PM UTC

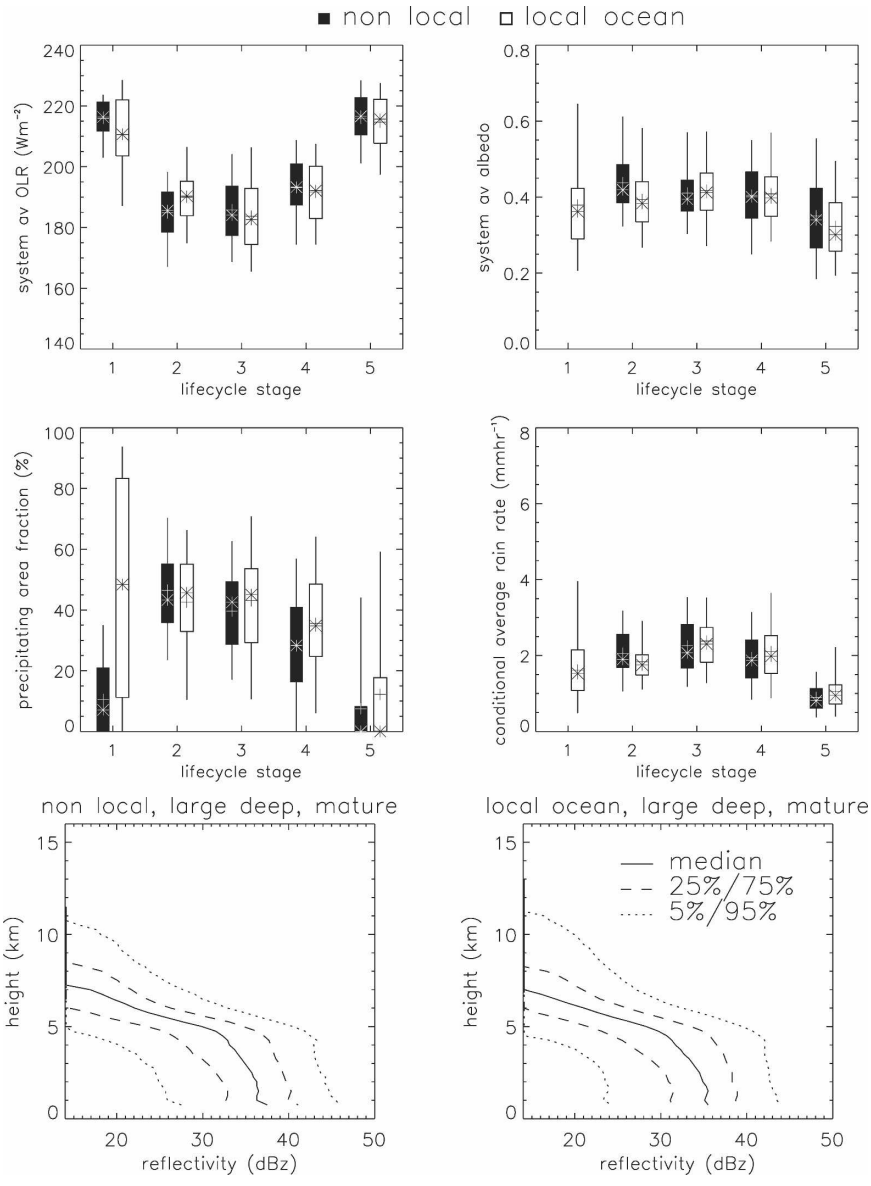

FIG. 9. Box and whisker plot of radiative [(top left) OLR and (top right) albedo] and precipitation properties [(bottom left) precipitation area fraction and (bottom right) conditional average rain rate] for "local" and "nonlocal" large deep Atlantic convective systems. Also shown are median and quartile profiles for convective regions of mature local and nonlocal Atlantic convective systems.

systems may be considered oceanic relatively close to the coastline. This may explain why the small number of nonlocal systems observed in the earliest stages of development (when they have just moved away from the coast) behave more similarly to land systems, with lower precipitating fractions than local ocean systems. However, this "memory" of their land-based development is short lived; comparison with Fig. 4 shows that while African systems are significantly deeper, brighter, and have smaller precipitating areas than their Atlantic counterparts, once these systems move out over the ocean and away from the coast, they behave in a very similar manner to locally forming systems. This point is further emphasized by the similarity in the distribution of convective profiles for the mature stage of the local and nonlocal oceanic systems.

7. Discussion

Taken together, our results suggest a fundamental difference in the evolution of large deep convective

Unauthenticated | Downloaded 03/24/25 02:03 PM UTC

clusters over land and ocean (at least between the African continent and Atlantic ITCZ). Over land, systems transition to more stratiform behavior over the system life cycle. Over ocean, however, the convective rain fraction and depth of convection remain essentially constant as the system grows, deepens, and begins to dissipate (as determined from the infrared signature). In the following sections we discuss possible reasons for this difference in behavior and investigate the importance of the convective intensity in determining the properties of the ensuing anvil clouds.

a. The role of sustainability and the diurnal cycle

The "sustainability" of an environment, that is, the ability to continually generate and sustain new convective cells, has previously been suggested to control the size of convective systems (Yuter and Houze 1998; Houze 2004) and their stratiform rain fraction (Schumacher and Houze 2003a, 2006). Since much of the stratiform rain observed in convective regions comes from regions of older, decaying convection (Houze 1997), the evolution of the system is largely governed by the balance between the formation of new active cells and the dissipation of older decaying cells.

Schumacher and Houze (2003a, 2006) suggested that the higher stratiform rain fraction observed over oceanic regions is due to a greater sustainability, with the warm moist boundary layer favoring the continual generation of moderately strong convection throughout the day and night. Over land, in comparison, they suggest that the strong diurnal cycle of surface heating triggers intense, daytime deep convection but that nocturnal cooling of the land surface limits the ability of the environment to support continued convective activity or to form new convection. Schumacher and Houze do however note that, in some situations, particularly where constrained by topography, a low-level moist jet may increase the sustainability over land at night.

The time of day at which African systems are observed in each life cycle stage (Fig. 10) confirms that even the longer-lived large deep systems reach maturity around midnight and dissipate through the morning hours, consistent with previous studies (e.g., Desbois et al. 1988; Liang and Fritsch 1993). However, as noted earlier, a subset of the systems excluded from our analysis do appear to persist through the night and regenerate the following afternoon. Large deep systems appear to form earlier in the day than smaller systems, although this may be an artifact of the assumption that the larger (and hence presumably older) system continues in a merger. System lifetimes for large deep systems are generally between 12 and 36 h with lifetimes of around 24 h occurring most frequently.

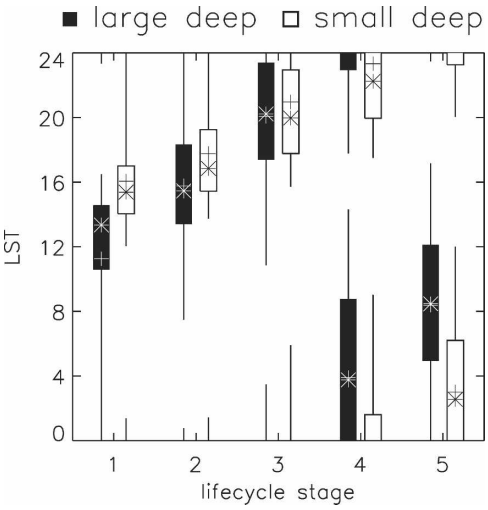

FIG. 10. Box–whisker plot showing local time of occurrence of each life cycle stage for large and small deep African systems.

While strong diurnal forcing from surface heating clearly plays a role in the preferential initiation of convection in the early afternoon, many other factors (such as orography and synoptic-scale forcings) are important in the organization and development of the mesoscale systems considered here (e.g., Mohr and Thorncroft 2006). As noted by Schumacher and Houze (2006), the monsoon circulation may also help to sustain convective systems through the night over West Africa during summer, limiting the impact of nocturnal surface cooling. The monsoon flow strengthens after sunset (Parker et al. 2005), pumping warm moist air into the boundary layer and helping to sustain a moderate level of convective activity during the night. This may explain why systems continue to grow after sunset and only reach their maximum extent around midnight (Fig. 10), and may contribute to the nocturnal regeneration sometimes observed in the subset of systems excluded from this study (see section 2b). However, systems begin to dissipate in the early morning hours, when the monsoon flow is at its strongest, suggesting that the enhancement of sustainability provided by the nocturnal jet is not sufficient to fully counteract the less favorable surface forcing. After sunrise turbulent mixing weakens the mean flow and dries the boundary layer (Parker et al. 2005), and any remaining convective activity usually ceases.

Over ocean, the diurnal cycle (not shown) is weak and difficult to separate from noise in the data. Large deep systems appear to form preferentially in the evening, but mature and dissipating systems occur with similar frequency at all times. This is consistent with behavior observed by Mapes (1993) and Chen et al.

Unauthenticated | Downloaded 03/24/25 02:03 PM UTC

(1996) in the western tropical Pacific. Small deep systems also develop preferentially in the late evening, reaching maturity in the early morning and dissipating most frequently around noon, consistent with previous studies (e.g., Yang and Slingo 2001).

The differences in evolution observed here for African and Atlantic systems are consistent with the differences in behavior predicted by Schumacher and Houze (2006) based on the sustainability hypothesis. Over ocean, or in other regions of high sustainability, new convective cells are continually generated and the systems begin to dissipate (decrease in extent) as the number, and depth, of cells that can be supported decreases, but the convective fraction remains essentially constant. Over land, or other regions where convection is strongly forced by the diurnal cycle, conditions are less favorable for the formation of new convective cells at night, leading to a more rapid decrease in convective activity and a transition to more stratiform behavior in the dissipating stages of the system's evolution.

b. *Dependence of system properties on convective intensity*

To our knowledge, only occasional direct measurements of the intensity of convection, such as updraft speed measurements, have been reported for the African region (Chong et al. 1987; Roux 1988). However, the information generated by the tracking algorithm allows an indirect estimate to be made. Sikdar and Suomi (1971) and Suchman et al. (1977) used the areal expansion rate of the upper-level cloud shield to estimate the convective mass transport from time-lapse satellite images. We make a similar estimate by using the polynomial curves fitted to the time series of system radius (section 2b) to calculate the area expansion rate

$$A_e = \frac{1}{A}\frac{\partial A}{\partial t}$$

(Machado et al. 1998; Machado and Laurent 2004), which we use to produce an estimate of the convective intensity.

We define a convective intensity index as $I_{\text{conv}} = \overline{A_e}\,\Delta z$, where Δz is the depth of the detraining layer and $\overline{A_e}$ is the average expansion rate during the developing stage. Here Δz is estimated as the difference between the height of the climatological melting layer (4.5 km) and the cloud top height. The latter is found from the temperature of the coldest GERB footprint using the seasonal and regional mean profile from the NCEP reanalysis. This index has units of meters per second but cannot be directly related to the vertical velocity within the cloud since condensation effects are not accounted for (Machado and Laurent 2004).

As can be seen in Fig. 11, both the modal and maximum values of the convective intensity index are roughly a factor of 2–3 higher over the African region than the Atlantic region. This is qualitatively consistent with the 2–3 times larger cumulus updraft velocities observed for continental convection during the Thunderstorm Project than in oceanic field campaigns (Zipser and Lutz 1994) and with the differences in mesoscale circulation strength reported by Houze (1989). The differences are also consistent with the well-known land–ocean contrast in other proxies for convective intensity, such as lightning occurrence and ice scattering (e.g., Cecil et al. 2005; Zipser et al. 2006). Figure 12 also shows a reasonable correlation, for storm heights of less than 10 km, between the convective intensity index and the depth of convective radar echoes, which is often used as a proxy for convective intensity. These results suggest that, within the population of systems considered here (cloud tops colder than 235 W m^{-2} for >3 h), more intense storms are, on average, deeper, larger, and longer lived than weaker storms, although the relationships with intensity break down for the most intense systems. The intensity may therefore be a useful statistical predictor of eventual system size for deep convective systems in GCMs that do not resolve the mesoscale. No clear relationship exists between the system albedo and the convective intensity or convective depth (not shown).

As was noted in section 4, convective profiles observed for large and small deep systems are very similar. This lack of correlation between system size and convective storm height is confirmed in Fig. 12. Similarly, cloud top temperature only weakly depends on the depth of the radar echo top for systems with convective storm height of more than 5 km. As might be expected (e.g., Zipser and Lutz 1994), the peak (and system averaged, not shown) lightning flash rate increases with the depth of the radar echoes in the convective region of the storm (Fig. 12).

8. Summary and conclusions

TRMM radar and lightning observations are matched to a database of tracked storms for which the life cycle stage has been determined from the evolution of the system size and minimum brightness temperature in geostationary satellite data. This provides a composite picture of the evolution of the vertical structure, rainfall, and lightning characteristics for mesoscale convective systems.

As found in previous studies (Machado and Rossow 1993; Boccippio et al. 2000; Toracinta and Zipser 2001; Schumacher and Houze 2003a, 2006), convective sys-

Unauthenticated | Downloaded 03/24/25 02:03 PM UTC

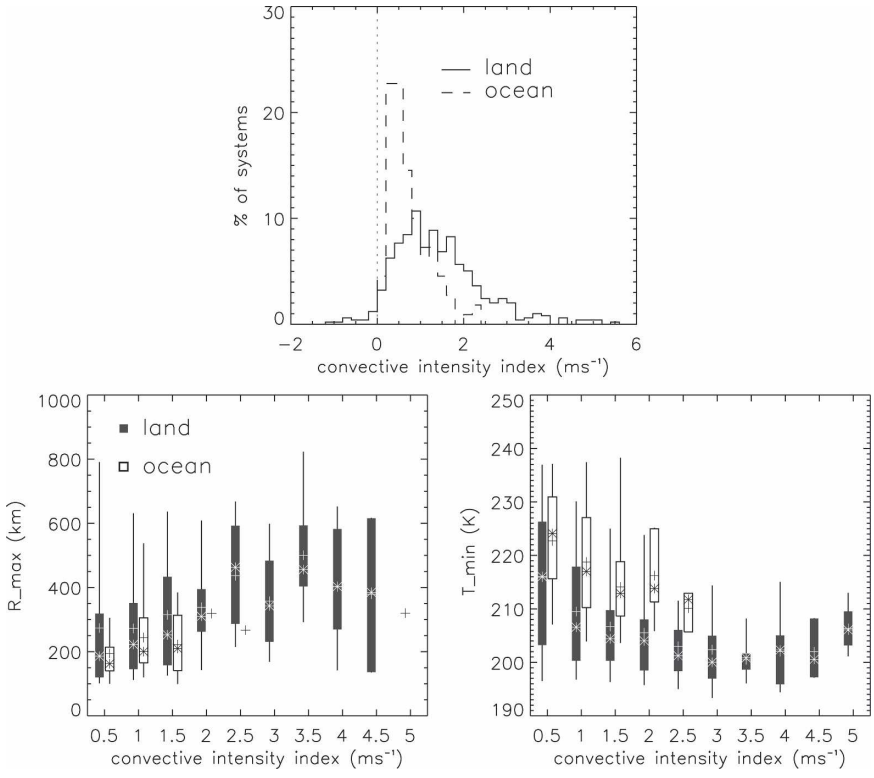

FIG. 11. Distribution of the convective intensity index I_{conv} for African and Atlantic convective systems. Also shown are box and whisker plots of the maximum system size (R_{max}) and the minimum brightness temperature (T_{min}) reached during the life cycle for 0.5 m s^{-1} bins of I_{conv}.

tems over Africa have colder cloud tops, higher albedo, deeper and more intense convection, and more frequent lightning, while larger and more heavily precipitating stratiform rain decks form in oceanic systems, resulting in larger precipitating area fractions over the Atlantic than over Africa. Analysis of systems propagating out over the West African coast suggest that system properties are determined by the local environment (continental versus maritime) rather than that in which the system initiated. If true in general, this would simplify the problem of representing these systems in climate models, as it means information on the origin of a system is not required to determine its behavior at a later stage of development.

Similar profiles of radar reflectivity are observed for convective cells during the mature stages of both small and larger deep convective systems, suggesting that the depth of convection does not directly control the horizontal extent of the system. The size, lifetime, and cloud top temperature are, however, correlated to some extent with the intensity of the convection, estimated here from the areal expansion rate.

African systems peak in convective activity early in their development with rainfall becoming more stratiform in nature as they evolve. In contrast, oceanic systems appear to show little variation in the convective rain fraction over their lifetime, despite a clear evolution in system size, depth, and precipitation fraction. Although infrequent, lightning activity also peaks late in the life cycle, after the maximum system size has been reached.

These differences in evolution are consistent with the hypothesis of greater convective sustainability over ocean (Yuter and Houze 1998; Schumacher and Houze 2003a, 2006; Houze 2004). According to this idea, new convective cells are continually generated over ocean and the life cycle is controlled by the balance between the rate at which new cells form and old ones dissipate. Over land, the strong diurnal forcing drives intense deep convection during the day, but conditions become less favorable for the initiation of new convection at night. Systems mature near midnight and convective cell initiation gradually decreases thereafter, leaving a predominantly stratiform decaying anvil cloud to dissipate after sunrise. Enhanced nocturnal sustainability related to the low-level monsoon flow over West Africa

Unauthenticated | Downloaded 03/24/25 02:03 PM UTC

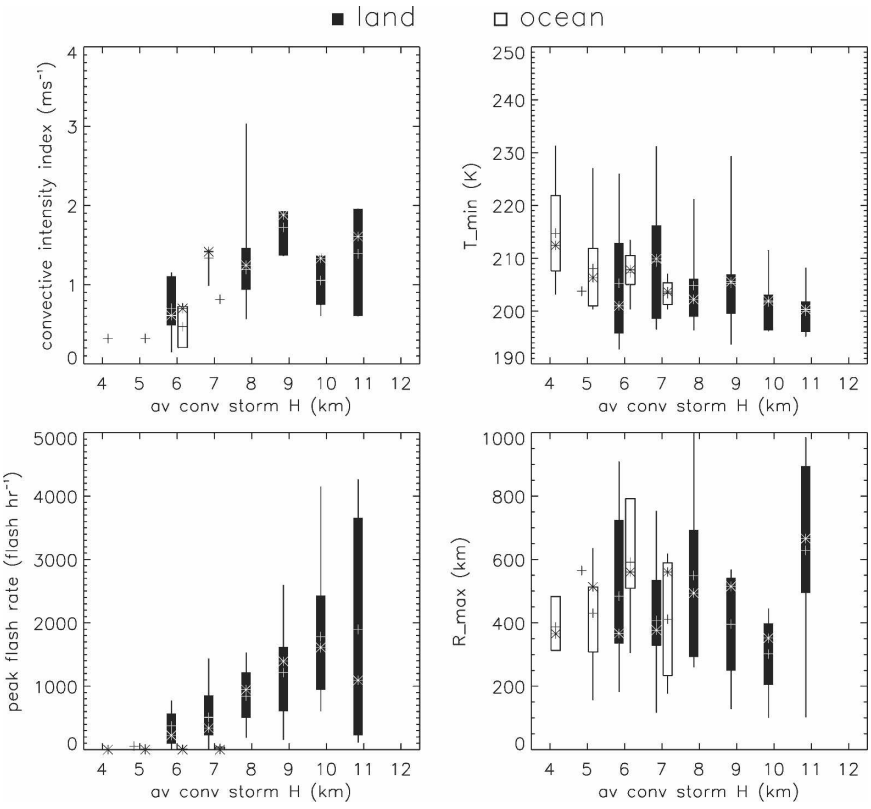

FIG. 12. Box and whisker plots of the convective intensity index, the minimum brightness temperature (T_{min}), the storm maximum flash rate and the maximum system size (R_{max}) reached for 1-km bins of the convective region storm height (height of the 17-dBZ contour of radar reflectivity) for systems observed by PR during the developing stage.

may contribute to the continued growth of land-based systems after sunset and may explain the occasional nocturnal regeneration of convection.

These results are based on a relatively small population of systems for one region of the Tropics and one season, and further investigation is required to assess their generality. Nevertheless, the observed differences in behavior have potentially important ramifications for the parameterization of convection and anvil cloud processes in climate models. Most current schemes generate convection in response to local instability, with detrained moisture passed to the large-scale cloud scheme to generate anvil regions. This is likely to produce behavior more akin to the observed evolution over land, with residual stratiform anvils left behind once the convective instability is used up, although the lack of mesoscale uplift may mean these anvils are not maintained for a sufficient duration. In contrast, our results suggest that over ocean (or at least the Atlantic ITCZ region), significant convective and stratiform rainfall throughout the system life cycle and that the system dissipates relatively rapidly once convection ceases. Thus, proper simulation of the oceanic life cycle may depend on assumptions about the adjustment time scale for the consumption of available convective potential energy.

Acknowledgments. TRMM PR and 3B42 data were obtained from the NASA Goddard DAAC and LIS data from the Global Hydrology Resource Center. GERB-like data were kindly provided by Nicolas Clerbaux at the Royal Meteorological Institute of Belgium (RMIB). We are grateful to Prof. Ed Zipser, Prof. Robert Houze Jr., and one anonymous reviewer for constructive comments, which greatly improved the original manuscript. This research was supported by the NASA Precipitation Measurement Missions Program.

REFERENCES

Aspliden, C. I., Y. Tourre, and J. B. Sabine, 1976: Some climatological aspects of West African disturbance lines during GATE. *Mon. Wea. Rev.,* **104,** 1029–1035.

Awaka, J., T. Iguchi, H. Kumagai, and K. Okamoto, 1997: Rain type classification algorithm for TRMM precipitation radar. *IEEE Trans. Geosci. Remote Sens.,* **4,** 1633–1635.

Unauthenticated | Downloaded 03/24/25 02:03 PM UTC

Boccippio, D. J., S. J. Goodman, and S. Heckman, 2000: Regional differences in tropical lightning distributions. *J. Appl. Meteor.,* **39,** 2231–2248.

Boer, E. R., and V. Ramanathan, 1997: Lagrangian approach for deriving cloud characteristics from satellite observations and its implications to cloud parameterization. *J. Geophys. Res.,* **102,** 21 383–21 399.

Cecil, D. J., S. J. Goodman, D. J. Boccippio, E. J. Zipser, and S. W. Nesbitt, 2005: Three years of TRMM precipitation features. Part I: Radar, radiometric, and lightning characteristics. *Mon. Wea. Rev.,* **133,** 543–566.

Chen, S. S., R. A. Houze Jr., and B. E. Mapes, 1996: Multiscale variability of deep convection in relation to large-scale circulation in TOGA COARE. *J. Atmos. Sci.,* **53,** 1380–1409.

Chong, M., P. Amayenc, G. Scialom, and J. Testud, 1987: A tropical squall line observed during the COPT 81 experiment in West Africa. Part I: Kinematic structure inferred from dual-doppler radar data. *Mon. Wea. Rev.,* **115,** 670–694.

Chou, C., and J. D. Neelin, 1999: Cirrus detrainment–temperature feedback. *Geophys. Res. Lett.,* **26,** 1295–1298.

Christian, H. J., 1999: Optical detection of lightning from space. *Proc. 11th Int. Conf. on Atmospheric Electricity,* Guntersville, AL, International Commission on Atmospheric Electricity, 715–718.

——, and J. Latham, 1998: Satellite measurements of global lightning. *Quart. J. Roy. Meteor. Soc.,* **124,** 1771–1773.

Clerbaux, N., and S. Dewitte, 1999: RGP-SP: Spectral modelling. RMIB Tech. Rep. MSG–RMIB–GE–TN–0005, 44 pp.

——, ——, L. Gonzarlez, C. Bertrand, B. Nicula, and A. Ipe, 2003: Outgoing longwave flux estimation: Improvement of angular modelling using spectral information. *Remote Sens. Environ.,* **85,** 389–395.

Del Genio, A. D., W. Kovari, M.-S. Yao, and J. Jonas, 2005: Cumulus microphysics and climate sensitivity. *J. Climate,* **18,** 2376–2387.

Desbois, M., T. Kayiranga, B. Gnamien, S. Guessous, and L. Picon, 1988: Characterization of some elements of the Sahelian climate and their interannual variations for July 1983, 1984 and 1985 from the analysis of METEOSAT ISCCP data. *J. Climate,* **1,** 867–904.

Futyan, J. M., J. E. Russell, and J. E. Harries, 2005: Determining cloud forcing by cloud type from geostationary satellite data. *Geophys. Res. Lett.,* **32,** L08807, doi:10.1029/2004GL022275.

Geerts, B., and T. Dejene, 2005: Regional and diurnal variability of the vertical structure of precipitation systems in Africa based on spaceborne radar data. *J. Climate,* **18,** 893–916.

Hartmann, D. L., and K. Larson, 2002: An important constraint on tropical cloud–climate feedback. *Geophys. Res. Lett.,* **29,** 1951, doi:10.1029/2002GL015835.

Hirose, M., and K. Nakamura, 2004: Spatiotemporal variation of the vertical gradient of rainfall rate observed by the TRMM precipitation radar. *J. Climate,* **17,** 3378–3397.

Hodges, K. I., and C. D. Thorncroft, 1997: Distribution and statistics of African mesoscale convective weather systems based on the ISCCP Meteosat imagery. *Mon. Wea. Rev.,* **125,** 2821–2837.

Houze, R. A., Jr., 1989: Observed structure of mesoscale convective systems and implications for large scale heating. *Quart. J. Roy. Meteor. Soc.,* **115,** 425–461.

——, 1997: Stratiform precipitation in regions of convection: A meteorological paradox? *Bull. Amer. Meteor. Soc.,* **78,** 2179–2196.

——, 2004: Mesoscale convective systems. *Rev. Geophys.,* **42,** RG4003, doi:10.1029/2004RG000150.

——, and C.-P. Cheng, 1977: Radar characteristics of tropical convection observed during GATE: Mean properties and trends over the summer season. *Mon. Wea. Rev.,* **105,** 964–980.

——, and A. K. Betts, 1981: Convection in GATE. *Rev. Geophys. Space Phys.,* **19,** 541–576.

——, and E. N. Rappaport, 1984: Air motions and precipitation structure of an early summer squall line over the eastern tropical Atlantic. *J. Atmos. Sci.,* **41,** 553–574.

Huffman, G. J., and Coauthors, 1997: The global precipitation climatology project (GPCP) combined precipitation dataset. *Bull. Amer. Meteor. Soc.,* **78,** 5–20.

Iguchi, T., T. Kozu, R. Meneghini, J. Awaka, and K. Okamoto, 2000: Rain-profiling algorithm for the TRMM precipitation radar. *J. Appl. Meteor.,* **39,** 2038–2052.

Kalnay, E., and Coauthors, 1996: The NCEP/NCAR 40-Year Reanalysis Project. *Bull. Amer. Meteor. Soc.,* **77,** 437–471.

Kozu, T., and Coauthors, 2001: Development of precipitation radar onboard the Tropical Rainfall Measuring Mission (TRMM) satellite. *IEEE Trans. Geosci. Remote Sens.,* **39,** 102–116.

LeMone, M. A., and E. J. Zipser, 1980: Cumulonimbus vertical velocity events in GATE. Part I: Diameter, intensity and mass flux. *J. Atmos. Sci.,* **37,** 2444–2457.

Liang, A. G., and J. M. Fritsch, 1993: Mesoscale convective complexes in Africa. *Mon. Wea. Rev.,* **121,** 2254–2263.

Lindzen, R. S., M.-D. Chou, and A. Y. Hou, 2001: Does the Earth have an adaptive infrared iris? *Bull. Amer. Meteor. Soc.,* **82,** 417–432.

Loeb, N. G., N. Manalo-Smith, S. Kato, W. F. Miller, S. K. Gupta, P. Minnis, and B. A. Wielicki, 2003: Angular distribution models for top-of-atmosphere radiative flux estimation from the clouds and the earth's radiant energy system instrument on the tropical rainfall measuring mission satellite. Part I: Methodology. *J. Appl. Meteor.,* **42,** 240–265.

Lucas, C., E. J. Zipser, and M. A. LeMone, 1994: Vertical velocity in oceanic convection off tropical Australia. *J. Atmos. Sci.,* **51,** 3183–3193.

Machado, L. A. T., and W. B. Rossow, 1993: Structural characteristics and radiative properties of tropical cloud clusters. *Mon. Wea. Rev.,* **121,** 3234–3260.

——, and H. Laurent, 2004: The convective system area expansion over Amazonia and its relationship with convective system life duration and high-level wind divergence. *Mon. Wea. Rev.,* **132,** 714–725.

——, W. B. Rossow, R. L. Guedes, and A. W. Walker, 1998: Life cycle variations of mesoscale convective systems over the Americas. *Mon. Wea. Rev.,* **126,** 1630–1654.

Mapes, B. E., 1993: Gregarious tropical convection. *J. Atmos. Sci.,* **50,** 2026–2037.

——, and R. A. Houze Jr., 1993: Cloud clusters and superclusters over the oceanic warm pool. *Mon. Wea. Rev.,* **121,** 1398–1415.

Martin, D. W., and A. J. Schreiner, 1981: Characteristics of West African and East Atlantic cloud clusters: A survey from GATE. *Mon. Wea. Rev.,* **109,** 1671–1688.

Mathon, V., and H. Laurent, 2001: Life cycle of Sahelian mesoscale convective cloud systems. *Quart. J. Roy. Meteor. Soc.,* **127,** 377–406.

——, A. Diedhiou, and H. Laurent, 2002: Relationship between easterly waves and mesoscale convective systems over the Sahel. *Geophys. Res. Lett.,* **29,** 1216, doi:10.1029/2001GL014371.

McCollum, J. R., A. Gruber, and M. B. Ba, 2000: Discrepancy

Unauthenticated | Downloaded 03/24/25 02:03 PM UTC

between gauges and satellite estimates of rainfall in equatorial Africa. *J. Appl. Meteor.,* **39,** 666–679.

Mohr, K. L., and C. D. Thorncroft, 2006: Intense convective systems in West Africa and their relationship to the African easterly jet. *Quart. J. Roy. Meteor. Soc.,* **132,** 163–176.

Nesbitt, S. W., E. J. Zipser, and D. J. Cecil, 2000: A census of precipitation features in the Tropics using TRMM: Radar, ice scattering, and lightning observations. *J. Climate,* **13,** 4087–4106.

Orville, R. E., and R. W. Henderson, 1986: Global distribution of midnight lightning: September 1977 to August 1978. *Mon. Wea. Rev.,* **114,** 2640–2653.

Parker, D. J., and Coauthors, 2005: The diurnal cycle of the West African monsoon circulation. *Quart. J. Roy. Meteor. Soc.,* **131,** 2839–2860.

Payne, S. W., and M. M. McGarry, 1977: The relationship of satellite inferred convective activity to easterly waves over West Africa and the adjacent ocean during phase III of GATE. *Mon. Wea. Rev.,* **105,** 413–420.

Petersen, W. A., and S. A. Rutledge, 2001: Regional variability in tropical convection: Observations from TRMM. *J. Climate,* **14,** 3566–3586.

Ramanathan, V., and W. Collins, 1991: Thermodynamic regulation of ocean warming by cirrus clouds deduced from observations of the 1987 El Niño. *Nature,* **351,** 27–32.

Roca, R., and V. Ramanathan, 2000: Scale dependence of monsoonal convective systems over the Indian Ocean. *J. Climate,* **13,** 1286–1298.

Rosenfeld, D., and I. M. Lensky, 1998: Satellite-based insights into precipitation formation processes in continental and maritime convective clouds. *Bull. Amer. Meteor. Soc.,* **79,** 2457–2476.

Roux, F., 1988: The West African squall line observed on 23 June 1981 during COPT 81: Kinematics and thermodynamics of the convective region. *J. Atmos. Sci.,* **45,** 406–426.

Rutledge, S. A., E. R. Williams, and T. D. Keenan, 1992: The down under Doppler and electricity experiment (DUNDEE): Overview and preliminary results. *Bull. Amer. Meteor. Soc.,* **73,** 3–16.

Schumacher, C., and R. A. Houze Jr., 2003a: Stratiform rain in the Tropics as seen by the TRMM precipitation radar. *J. Climate,* **16,** 1739–1756.

——, and ——, 2003b: The TRMM precipitation radar's view of shallow, isolated rain. *J. Appl. Meteor.,* **42,** 1519–1524.

——, and ——, 2006: Stratiform precipitation production over sub-Saharan Africa and the tropical East Atlantic as observed by TRMM. *Quart. J. Roy. Meteor. Soc.,* **132,** 2235–2255.

Sherwood, S. C., and R. Wahrlich, 1999: Observed evolution of tropical deep convective events and their environment. *Mon. Wea. Rev.,* **127,** 1777–1795.

——, V. T. J. Phillips, and J. S. Wettlaufer, 2006: Small ice crystals and the climatology of lightning. *Geophys. Res. Lett.,* **33,** L05804, doi:10.1029/2005GL025242.

Sikdar, D. N., and V. E. Suomi, 1971: Time variation of tropical energetics as viewed from a geostationary altitude. *J. Atmos. Sci.,* **28,** 170–180.

Suchman, D., D. W. Martin, and D. N. Sikdar, 1977: Deep convective mass transports: An estimate from a geostationary satellite. *Mon. Wea. Rev.,* **105,** 943–955.

Thompson, R. M., Jr., S. W. Payne, E. E. Recker, and R. J. Reed, 1979: Structure and properties of synoptic-scale wave disturbances in the intertropical convergence zone of the eastern Atlantic. *J. Atmos. Sci.,* **36,** 53–72.

Toracinta, E. R., and E. J. Zipser, 2001: Lightning and SSM/I-ice-scattering mesoscale convective systems in the global Tropics. *J. Appl. Meteor.,* **40,** 983–1002.

——, D. J. Cecil, E. J. Zipser, and S. W. Nesbitt, 2002: Radar, passive microwave, and lightning characteristics of precipitating systems in the Tropics. *Mon. Wea. Rev.,* **130,** 802–824.

Wilcox, E. M., and V. Ramanathan, 2001: Scale dependence of the thermodynamic forcing of tropical monsoon clouds: Results from TRMM observations. *J. Climate,* **14,** 1511–1524.

Williams, E. R., and S. Stanfill, 2002: The physical origin of the land-ocean contrast in lightning activity. *C. R. Acad. Sci. Phys.,* **3,** 1277–1292.

Williams, M., and R. A. Houze Jr., 1987: Satellite-observed characteristics of winter monsoon cloud clusters. *Mon. Wea. Rev.,* **115,** 505–519.

Yang, G.-Y., and J. Slingo, 2001: The diurnal cycle in the Tropics. *Mon. Wea. Rev.,* **129,** 784–801.

Yuter, S. E., and R. A. Houze Jr., 1995: Three-dimensional kinematic and microphysical evolution of Florida cumulonimbus. Part II: Frequency distributions of vertical velocity, reflectivity, and differential reflectivity. *Mon. Wea. Rev.,* **123,** 1941–1963.

——, and ——, 1998: The natural variability of precipitating clouds over the western Pacific warm pool. *Quart. J. Roy. Meteor. Soc.,* **124,** 53–99.

Zipser, E. J., 1994: Deep cumulonimbus cloud systems in the Tropics with and without lightning. *Mon. Wea. Rev.,* **122,** 1837–1851.

——, and K. R. Lutz, 1994: The vertical profile of radar reflectivity of convective cells: A strong indicator of storm intensity and lightning probability? *Mon. Wea. Rev.,* **122,** 1751–1759.

——, D. J. Cecil, C. Liu, S. W. Nesbitt, and D. P. Yorty, 2006: Where are the most intense thunderstorms on Earth? *Bull. Amer. Meteor. Soc.,* **87,** 1057–1071.

Unauthenticated | Downloaded 03/24/25 02:03 PM UTC